A Preliminary Study on the Solidification Cracking and Stress Relief Cracking Susceptibility of Various Compositions of 10 Weight Percent Nickel Steel

Nicholas Yang
2023

A Preliminary Study on the Solidification Cracking and Stress Relief Cracking Susceptibility of Various Compositions of 10 Weight Percent Nickel Steel

by

Nicholas Yang

A Thesis

Presented to the Graduate and Research Committee

of Lehigh University

in Candidacy for the Degree of

Master of Science

in

Materials Science and Engineering

Lehigh University

May 2023

Thesis is accepted and approved in partial fulfillment of the requirements for the Master of Science in (Major).

A PRELIMINARY STUDY ON THE SOLIDIFICATION CRACKING AND STRESS RELIEF CRACKING SUSCEPTIBILITY OF VARIOUS COMPOSITIONS OF 10 WEIGHT PERCENT NICKEL STEEL
NICHOLAS L. YANG

April 30th, 2023

Date Approved

John N. DuPont

Director/Advisor

Ricardo H. R. Castro

Department Chair/Second Reader

ACKNOWLEDGMENTS

I would like to thank my close friends and family for supporting my academic goals. Without them, I would not be where I am today. I would especially like to thank Dr. John DuPont for providing me the guidance and tools to strive for a profound education and being a reliable mentor throughout my graduate studies.

Table of Contents

LIST OF TABLES

LIST OF FIGURES

ABSTRACT

Research involving the mechanical properties of 10 weight percent nickel steel has recently exemplified its great ballistic resistance and toughness at low temperatures. These superior mechanical properties support the candidacy of this steel to be used in naval combatant ships and other military components that are exposed to low sea temperatures. Despite its potential uses for such applications, limited research has been conducted on the mechanical stability during and after welding, which is essential for the fabrication of military parts. During the weld thermal cycle, the heat affected zone of the steel becomes exposed to very high temperature changes over a short amount of time. This thermal gradient across the span of the HAZ subjects it to high internal stresses after welding. To relieve these stresses, a post-weld heat treatment must be employed, which requires plastic deformation at elevated temperatures. During this process, localized deformation along the grain boundaries can result in low ductility failures, a process known as stress-relief cracking. Another common failure mechanism in steel welds is called solidification cracking, which is a result of non-equilibrium solidification and solute segregation. The solidification cracking and stress-relief cracking susceptibility of three 10 weight percent nickel alloy with varying compositions was investigated using Gleeble, Varestraint, and microscopy techniques. The cracking susceptibility of HY-100, a well-established steel currently being used in ship hull material was also investigated and compared to the 10 weight percent nickel alloys. It was found that the stress relief cracking response largely depend on the carbon content and the post-weld heat treatment temperature, while the trends in solidification cracking susceptibility also depend on the content of tramp elements such as P and S, however further investigation will be necessary to confirm these trends. This investigation provides a reasonable approach to identifying the most suitable composition to be used in hull structure material while avoiding failure via these two mechanisms, and identifies a good post-weld heat treatment temperature to be used after welding this alloy.

1. INTRODUCTION

US Naval applications require steels with good resistance to fracture that are readily weldable. Previous work [1,2] led to the development of a steel with 10 wt% Ni (10 Ni) that utilizes the transformation induced plasticity (TRIP) effect for excellent toughness. More recent work [3-5] has been conducted to understand the phase transformations and mechanical properties that occur during welding of this new steel. The effects of welding thermal cycles on the mechanical properties the 10 Ni steel were studied using welding simulations to replicate microstructures observed in the heat-affected zone. The microstructural influences on austenite content, strength, and toughness were determined using a variety of characterization techniques including x-ray diffraction (XRD), scanning electron microscopy (SEM), electron backscatter diffraction (EBSD), and scanning transmission electron microscopy/energy dispersive spectroscopy (STEM/EDS). The results demonstrated that with increasing peak temperature of the welding thermal cycle, the amount of austenite present in the microstructure decreased. However, the toughness results did not directly correlate with the austenite contents. Poor toughness was observed in the intercritical heat-affected zone as a result of brittle high carbon martensite in this region. This region represents the greatest challenge in terms of maintaining high ballistic resistance of welds of 10 Ni steel. These results are significant in that the toughness of the HAZ in this steel is not solely based on the austenite content, which would be expected given it is a TRIP steel, but instead is a function of other microstructural influences. Similar characterization studies were conducted in the fusion zone and demonstrated that the toughness is largely controlled by the amount of oxides that form from oxygen absorption by the liquid weld pool [6,7].

The primary use of the newer 10 Ni steel will be as a welding filler metal for high strength steels such as HY-100. Full scale use of this new steel will require welds that are free of common metallurgical welding defects such as solidification cracks and stress relaxation cracks. However, no detailed information exists on the susceptibility of this new steel to solidification cracking or stress relief cracking. Thus, the objective of this work is to conduct preliminary solidification cracking and stress relief cracking

tests on three different heats of 10 Ni steel and compare the results to a currently used high strength steel, with primary emphasis being placed on the stress relief cracking behavior.

2. EXPERIMENTAL PROCEDURE

An HY-100 base metal plate was used to make gas metal arc welds (GMAW) using three different 10 Ni filler material compositions. The composition of each filler material and the HY-100 base material are shown in Table 1. Also shown are the compositions of 304 stainless steel (SS) and 310 SS used for comparative purposes in the solidification cracking studies. Table 2 shows the welding parameters used to make the welds. Twenty passes were made to fill each groove joint, as shown in Figure 1.

Testing of the 10 Ni samples was conducted by extracting specimens from the weld metal in the test plates. Therefore, the composition within the weld metal must be uniform to ensure that the weldability results are representative of the 10 Ni steel fusion zone. The uniformity of the weld metal was verified through the use of energy dispersive x-ray spectroscopy (EDS) to collect compositional traces across the cross-section of each weld. Figure 2 shows an example composition trace along a section of the weld made with the 11337 filler material. The Ni concentration was recorded because there is a significant difference in Ni concentration between the weld metal and base metal. The results show that the Ni concentration is relatively constant (between 9 to 10 wt%) in the weld metal, and reduces below 3 wt% Ni in the base metal outside of the fusion zone. Multiple compositional traces conducted across all the welds showed similar results, thus verifying that the weld metal composition was fairly uniform.

The stress relief cracking (SRC) susceptibility was determined using a Gleeble-based procedure previously described by Kant and DuPont and is briefly reviewed here [8]. As shown in Figure 3(a), the SRC samples were extracted from the welded plate, oriented perpendicular to the weld so that the weld metal was in the center of the sample.

Figure 3(b) shows the dimensions of the SRC samples. A thermocouple was welded to the center of the sample to record and control its temperature throughout the test.

Figure 4 shows the variation in temperature and stress with time during a typical SRC test [8]. The sample was heated up to 1250 ^{o}C to simulate the coarse grain heat affected zone (HAZ), followed by a rapid cool back down to room temperature. The sample was then heated up to a specified post weld heat treatment (PWHT) temperature and pulled to a strain of 1%. This strain level was used to ensure significant plastic deformation in each sample. The SRC sample was then held in place to permit stress relaxation until either failure occurred or eight hours. Samples that didn't fail during the eight hours of testing were pulled to failure at a strain rate between 1.90 and 1.98 mm s^{-1}. The SRC testing was done on all welds made with the three filler metals and the HY-100 base metal using four different PWHT temperatures of 400, 500, 600, and 700 ^{o}C.

Varestraint samples were removed from all weld metal samples with the following dimensions: 5.75" length x 1" width x 0.25" thickness. All the Varestraint tests were conducted at a torch travel speed of 2 mm s^{-1}, current of 200 A, and voltage of 12 V. Three to four samples of each alloy were tested using a three percent augmented strain. An AZ100 Light Optical Microscope (LOM) was used to gather images of each sample. The solidification cracking susceptibility of each alloy was determined by measuring the average maximum crack length (MCL). The direction of the largest crack was typically along the weld centerline. Differential Scanning Calorimetry (DSC) heating and cooling curves were conducted at a heating and cooling rate of 10 ^{o}C/minute to determine the solidification temperature range (STR) of each alloy.

3. RESULTS AND DISCUSSION

4.1 High Temperature Tensile Testing

In order to conduct the SRC tests, it is required to know the stress-strain response at each of the SRC test temperatures. This information is then used to control the extent of

applied strain and stress at each PWHT temperature used in the SRC test. Figure 5 shows the stress-strain curves of each alloy at temperatures of 400, 500, 600, and 700 ^{o}C. These results show that each alloy could safely be pulled to 1% strain during SRC testing without concern for necking or failure. Figure 6 shows the variation in tensile properties as a function of temperature for each alloy. As expected, the yield strength (YS) and ultimate tensile strength (UTS) decrease with increasing PWHT temperature.

4.2 SRC Test Results

Figure 7 shows the stress relaxation results at each of the PWHT temperatures. At 400 ^{o}C, failure only occurred for the HY-100 steel after about 2.5 hours (the total test period is eight hours, and samples are pulled to failure if failure has not occurred by that time). At 700 ^{o}C, none of the alloys failed within the eight-hour test. All the samples failed during stress relaxation at 500 ^{o}C, and only alloy 11705 did not fail in less than eight hours when tested at 600 ^{o}C. Thus, it is readily apparent that the cracking susceptibility is the highest at 500 and 600 ^{o}C.

Figure 8 shows how the PWHT temperature influences the failure time of each alloy, and Figure 9 compares the results for all the alloys. These failure curves exhibit a classic "C" shape, clearly showing the shortest failure times at intermediate PWHT temperatures of 500 ^{o}C and 600 ^{o}C. The shapes of these curves are similar to traditional time-temperature transformation (TTT) curves associated with precipitation that exhibit slow nucleation and growth kinetics at low and high temperatures, with nucleation and growth occurring the fastest at intermediate temperatures. The similarity between the "C" shaped failure curves and TTT diagrams is expected since the SRC susceptibility is typically closely linked to the precipitation kinetics.

At relatively low temperatures, the precipitation kinetics are sluggish due to low diffusivity. As a result, the alloy is not significantly strengthened by precipitation and retains ductility that permits stress relief by plastic deformation without fracture. Precipitation kinetics are sluggish at higher temperatures due to reduced driving force,

which also leaves the material in a relatively ductile state. This effect, combined with the higher temperature, also permits uniform stress relaxation by plastic deformation. At the intermediate temperatures of 500 and 600 ^{o}C, the precipitation kinetics are relatively fast and hardening is expected that inhibits stress relaxation by plastic deformation, leading to stress relief in the form of fracture. Figure 10 shows how the ductility of each alloy varies after exposure to the various PWHT temperatures. Note that the ductility is consistently the lowest at temperatures of 500 and 600 ^{o}C where the cracking susceptibility is the highest. Future work involving electron microscopy of the SRC samples would be useful to clarify the expected precipitation behavior and to identify the precipitates involved with premature SRC failure.

The failure curves are also useful from a practical sense to provide a guide for selection of PWHT temperatures and for ranking the cracking susceptibility among the alloys considered. In terms of PWHT temperatures, 500 and 600 ^{o}C should probably be avoided when possible, since all the alloys are most vulnerable to cracking within this temperature regime. While cracking susceptibility is relatively low for the alloys at 400 ^{o}C, the stress relaxation curves (Figure 7) show that there is not much stress relaxation at this lower temperature. A PWHT temperature of 700 ^{o}C is most efficient from a stress relaxation perspective. However, it is recognized that this would put the 10 Ni filler metal in the austenite/ferrite two phase regime and thus may not be practical. The comparative cracking susceptibilities between the HY-100 base metal and three filler metals may be useful in this regard. Note that the HY-100 base metal clearly exhibits the highest susceptibility to SRC cracking (Figure 9). The 10 Ni filler metal will be used to join high strength steels such as HY-100. Thus, as long as measures are taken during PWHT to prevent cracking in the HY-100, cracking would not be expected to occur in the weld metal when 10 Ni is used as a filler metal. Of the filler metals considered, alloy 11705 generally has the best resistance to SRC cracking as indicated by comparison of the failure curves shown in Figure 9.

The observed differences in cracking susceptibility among the alloys appear to be at least partially influenced by the differences carbon concentration and its associated effect on carbide precipitation. The HY-100 base metal has the highest carbon

concentration (0.17 wt %) and also the highest susceptibility to cracking. In contrast, the 11705 filler metal has the lowest carbon concentration (0.019 wt%) and is least susceptible to cracking. The 11337 (0.063 wt% C) and 11334 filler metals (0.096 wt% C) have intermediate carbon levels and also intermediate levels of cracking susceptibility. A higher carbon concentration results in increased super saturation beyond the solubility limit, which is the driving force for carbide precipitation. Thus, the amount and rate of carbide precipitation would be expected to scale with the nominal carbon concentration, and this likely accounts for at least some of the observed differences in cracking susceptibility among the alloys.

Figure 11 through Figure 14 show representative fracture surfaces of each sample from various PWHT temperatures. The fracture surface images were taken with a HITACHI 4300 SEM using the parameters listed in Table 3. At 400 ^{o}C, only the HY-100 steel failed by SRC during stress relaxation testing, and this is consistent with the intergranular fracture mode (Figure 11) that is commonly observed during SRC failure. The samples made from the 10 Ni filler metal did not fail after eight hours of stress relaxation at 400 ^{o}C and were thus pulled to failure. All these alloys exhibited evidence of plasticity as indicated by the micro void coalescence (MVC) fracture mode. Similar results are shown at the PWHT temperature of 700 ^{o}C (Figure 14), where all the samples survived the eight hour test without fracture and exhibited a MVC fracture mode when finally pulled to failure at the completion of the test. In contrast, all the samples exhibited significant amounts of intergranular fracture when tested at PWHT temperatures of 500 and 600 ^{o}C (Figure 12), and this is consistent with the short failure times observed for these conditions in the SRC test.

4.3 Relative Stress Relief Cracking Susceptibility

A procedure was recently developed that utilizes six measures of the SRC test results to quantitatively rank the cracking susceptibility of various alloys and PWHT temperatures. The procedure in described in detail elsewhere [8] and is briefly reviewed here. The six measures of SRC susceptibility include the time to failure, amount of stress

relaxed, ductility, increase in hardness during PWHT (relative to unaffected base metal), type of fracture mode, and nature of secondary cracking below the fracture. Higher susceptibility to SRC is correlated to reductions in the failure time, amount of stress relaxed, and ductility. An increase in hardness during PWHT would also indicate increased SRC susceptibility, as would the occurrence of intergranular cracking.

In terms of the fracture and secondary cracking mode, recent work [8] has shown that four different types of fracture modes and subsurface cracking can occur during SRC, depending on the susceptibility of the alloy and PHWT temperature. Type I and II fracture modes are intergranular with very low ductility. Type I fracture exhibits grain facets that are smooth with no evidence of significant localized plastic deformation. In contrast, the Type II fractures exhibit grain facets with microvoid coalescence (MVC), suggesting localized softening near the grain boundary. The Type III fracture mode is a mixed type of intergranular fracture and ductile MVC with moderate ductility. Thus, Type III fracture mode indicates moderate susceptibility to SRC. The Type IV fracture mode is completely ductile with MVC, which indicates that the alloy can accommodate plastic strain and hence is resistant to SRC.

Similarly, four major types of secondary cracks were observed below the fracture surface. Type I secondary cracks exhibit extensive intergranular cracking with equiaxed grains and low ductility. Minimal plastic deformation of the grains (as evident by the preserved equiaxed grain structure) with intergranular secondary cracks is indicative of cracking (instead of plastic deformation) being the active mechanism of stress relaxation. Hence, Type I secondary cracks indicate high SRC susceptibility. The Type II cracks are also rather sharp and intergranular, but with lower frequency than Type I cracks. In addition, samples with Type II cracks exhibit slightly increased plasticity (as indicated by the elongated grains) that is indicative of lower SRC susceptibility as compared to Type I. The Type III cracks are intergranular, but the cracks are rounded with evidence of blunting associated with appreciable plastic deformation. Finally, samples with Type IV cracks exhibit extensive plasticity (MVC) and no failure during the SRC test, thus show resistance to SRC under the test conditions.

The six measures of SRC susceptibility were combined with concepts of the Risk Priority Number (RPN) [8]. The RPN is a tool in Failure Modes and Effect Analysis (FMEA) used for risk assessment of various critical modes of failure for any design or process. In a manner similar to the RPN, the six measures of cracking susceptibility were combined to provide a Susceptibility Number (SN), where higher SN values correlate with higher cracking susceptibility. The value of SN is given by Equation 1, where SP_n represents the six susceptibility parameters from SP_1 to SP_6 for each SRC test, namely, ductility, percentage stress relaxed, increase in hardness at fracture (compared to base metal), failure time, fracture mode and secondary cracks below the fracture. The '*Severity*' and '*Detectability*' are respectively the severity and detectability values for each SP_n as discussed below.

$$SN = \sum_{SP_1}^{SP_6}(SP_n * Severity_n * Detectability_n) \qquad \text{Equation 1}$$

The assigned values of 'severity' and 'detectability' for all the susceptibility parameters (SP) are listed in Table 4. It is recognized that these values are somewhat subjective. However, with logical rationale for assigning the values, the extent of subjective nature can be reduced. Furthermore, results of a recent sensitivity analysis [8] show that reasonable variations to the parameters have minimal effect on the susceptibility ranking results, thus demonstrating the robustness of the approach.

A stronger indicator to SRC susceptibility was assigned a higher 'severity' value (maximum of 10). For example, the type of fracture mode is a stronger indicator as compared to hardness increase at fracture because intergranular fracture highlights SRC susceptibility irrespective of the alloy system. However, the increase in hardness near fracture is an inherent property of an alloy and can be due to both precipitation strengthening and/or work hardening. Detectability was defined as the confidence in the measured value of an SP. For example, the time to failure can be accurately measured during the stress relaxation tests, and thus was assigned a higher value as compared to the subjective parameters like fracture mode.

The fracture mode and secondary cracks are both qualitative parameters, hence, cannot be used directly in the SN calculation. Therefore, the major fracture modes and secondary crack types were assigned values out of 10 shown in Table 4, where a higher number indicates higher SRC susceptibility. The other SP values were also expressed out of 10 for consistency. The SP values for percent hardness increase were calculated by simply dividing the experimentally calculated value by 10. The SP values for ductility, failure time and stress relaxed (all values expressed as percentages) were calculated using the simple relation given by Equation 2. The complementary values of the three SP values (as calculated by Equation 2) were used in the SN calculation and not the values themselves because these SP hold an inverse relation with SRC susceptibility. For example, a higher value of ductility, percentage stress relaxed, or failure time indicate lower SRC susceptibility but result in a higher SN. Therefore, using the complementary values for these SP will maintain the direct relation to both SRC susceptibility and SN.

$$SP_n = (100 - SP_n)/10 \qquad \text{Equation 2}$$

For simplicity of plotting, the SN values (calculated using Equation 1) for the entire spectrum of samples and test conditions were normalized to the highest value in the series and multiplied by 100.

Figure 15 shows how SN value changes with alloy and PWHT temperature. The results provide a convenient approach for summarizing all the results of the SRC tests into a single value for comparative purposes. These results clearly show that all alloys exhibit the highest cracking susceptibility at 500 and 600 ^{o}C. Also note that the HY-100 base metal exhibits the highest cracking susceptibility among all the alloys at both temperatures. This is useful insight from a practical perspective because, as stated above, as long as measures are taken to avoid cracking in the base metal during PWHT, then cracking would not be expected in the weld metal made with the 10 Ni filler metals.

A PWHT temperature of 700 ^{o}C always provides the lowest cracking susceptibility, but this is subject to the limitations mentioned earlier concerning heating into the two phase austenite/ferrite phase field during PWHT.

4.4 Solidification Cracking

Figure 16 shows the average MCL for each alloy from the Varestraint tests. The 310 SS, an alloy that is moderately to highly susceptible to solidification cracking, and 304L SS, an alloy with very low solidification cracking susceptibility, were used for comparison [9]. Of the 10 Ni filler metals, the 11337 heat of 10 Ni exhibited the highest cracking susceptibility and was slightly higher than 310 stainless steels. This suggests that care should be taken when fusion welding of this alloy to minimize heat input and restraint in order to minimize the likelihood of cracking. The other two heats of 10 Ni steel (11705 and 11334) were similar to the HY-100 base metal. The HY-100 steel is readily fusion welded with very low risk of solidification cracking, so the 11705 and 11334 heats of 10 Ni steel would generally be considered readily weldable from a solidification cracking perspective.

DSC tests were conducted in attempt to measure the solidification temperature range (STR) of each alloy since the STR is well known to have a significant effect on susceptibility to solidification cracking [10]. Alloys with a relatively wide STR will exhibit a large solid + liquid mushy zone behind the liquid weld pool where solidification cracking occurs. When this occurs, there is a relatively large region within the low temperature portion of the mushy zone that contains small amounts of liquid that can wet the interdendritic and grain boundary regions, thus making the support of residual strains from thermal contraction and solidification difficult, and this is where cracking occurs. In this view, the formation of secondary phases from the solute rich liquid that may form at low temperature are known to be particularly detrimental to solidification cracking. Figure 17 shows typical heating and cooling DSC results for each alloy. The STR for fusion welds is represented by the difference between the on-heating liquidus temperature and the terminal solidus temperature determined from the

cooling scans. The on-heating liquidus temperature is used from DSC results because it does not exhibit undercooling effects that occur during the cooling portion of the DSC scan, and this is representative of the epitaxial growth that occurs at the fusion line in welds that also does not involve undercooling. The on-cooling terminal solidus is used since this is representative of the low temperature secondary phases that form from the solute rich interdendritic liquid.

Reference to the DSC results for alloy 11337 in Figure 17 shows that it exhibits a liquidus temperature of 1526 ^{o}C and a terminal solidus temperature of 1399 ^{o}C, with a corresponding STR of 127 ^{o}C. In comparison, the HY-100 base metal exhibits a liquidus of 1526 ^{o}C, terminal solidus of 1426 ^{o}C, and a slightly lower STR (relative to 1137) of 100 ^{o}C. This difference in STR would at least partially account for the observed differences in cracking susceptibility between these two alloys. No secondary low temperature peaks were observed in the cooling DSC scans for the 11334 and 11705 alloys. However, it is important to note that the absence of peaks in the DSC scan does not confirm that low temperature reactions did not occur. Secondary phases that form in very small amounts may not give off enough thermal energy to be detectable during DSC testing. Additional DSC testing, perhaps with larger samples, would be required to detect possible low temperature solidification reactions and their potential effect on solidification cracking tendency.

In terms of composition, solidification cracking of steels can be affected by the primary solidification mode and amount of tramp elements such as P and S. Alloys that solidify in the primary austenite mode are well known to be more susceptible to cracking than alloys that solidify as primary ferrite [11]. This difference is generally associated with variations in the relative solubility of P and S in the austenite and ferrite phases. The enhanced solubility of P and S in ferrite permits more of these tramp elements to be retained in solution during solidification, thus minimizing the segregation to the interdendritic liquid where very low melting point sulfides and phosphides can form that are known to be detrimental to solidification cracking. The Mn concentration can also play a role due to its ability to tie up S and thus minimize the detrimental influence of S. Recent solidification simulations have shown that the 10 Ni steel solidifies in the

primary austenitic mode [1], and this may at least partially account for the similarity in cracking response between the 11337 heat of 10 Ni and 310 SS shown in Figure 16. It is difficult to draw any additional definitive information on the role of composition when comparing the relative cracking susceptibility of the 10 Ni alloys. Reference to the compositions shown in Table 1 reveals that the 11334 heat has the lowest P and S concentrations and also exhibits the best resistance to cracking among the 10 Ni alloys. The 11705 heat has higher amounts P and S that the 11334 heat, but the amounts of P and S are similar to that of the 11337 heat that had the poorest resistance to cracking. However, the 11705 heat also has the highest amount of Mn of the heats considered, and this may have effectively minimized the deleterious effects of the relatively high P and S concentrations. The formation of the low temperature P-rich and S-rich phases that can cause cracking are typically very fine and difficult to characterize accurately with conventional scanning electron microscopy techniques. Additional work by transmission electron microscopy (TEM) would be needed to more clearly elucidate the possible of roll of composition differences and associated differences in cracking tendency among the 10 Ni heats considered here.

4. CONCLUSIONS AND FUTURE WORK

A preliminary study was conducted to determine the relative SRC and solidification cracking susceptibility of four different alloys, namely 10 Ni samples of heats 11334, 11337, and 11705, and HY-100 base material. The following conclusions can be drawn from these results:

1. The SRC susceptibility of all three 10 Ni filler metals was lower than that of the HY-100 base metal. Thus, as long as measures are taken to avoid SRC cracking in the HY-100 base metal during PWHT, then cracking would not be expected to occur in the fusion zone when any of the 10 Ni steels are used as filler metals.

2. The SRC susceptibility was the highest at PWHT temperatures at 500 and 600 ^{o}C for all the alloys considered. Little to no cracking was observed at PWHT temperatures of 400 and 700 ^{o}C. The variation in cracking susceptibility with PWHT temperature is likely associated with variations in the carbide precipitation kinetics that are probably the fastest at temperatures of 500 and 600 ^{o}C.
3. The observed differences in SRC susceptibility among the alloys appear to be at least partially influenced by differences in carbon concentration and its associated effect on carbide precipitation kinetics. The HY-100 base metal had the highest carbon concentration and the highest susceptibility to cracking, while the 11705 filler metal has the lowest carbon concentration and was least susceptible to cracking. The 11337 and 11334 filler metals had intermediate carbon levels and also intermediate levels of cracking susceptibility.
4. The 11334 and 11705 filler metals and HY-100 base material all exhibited similar maximum crack lengths during Varestraint testing. Experience shows that the HY-100 steel is readily weldable from a solidification cracking viewpoint, so the 11334 and 11705 filler metals would also expect to be readily weldable. The 11337 filler metal had the highest solidification cracking susceptibility of all the alloys considered, which may be associated with its relatively high P and S and moderate Mn concentrations.
5. Additional microstructural characterization by transmission electron microscopy (TEM) would be useful to more clearly elucidate the roll of alloy composition on the SRC and solidification cracking susceptibility of these alloy. TEM of the SRC samples would be useful for understanding how grain boundary carbide phases may be influencing the SRC cracking tendency. Similarly, TEM of the Varestraint samples would be useful for identifying any solute rich secondary phases (such as sulfides and phosphides) that may be influencing the susceptibility to solidification cracking.

REFERENCES

1. Barrick, E., 2016. *Fundamental Studies of Phase Transformations and Mechanical Properties in the Heat Affected Zone of 10 wt% Nickel Steel*. Ph.D. Lehigh University.
2. Nippes, E. and Balaguer, J., 1985. a study of the weld heat-affected zone toughness of 9% nickel steel. pp.237-243.
3. Divya Jain, David N. Seidman, Erin J. Barrick, John N. DuPont, Atom-Probe Tomographic Investigation of Austenite Stability and Carbide Precipitation in a TRIP-assisted 10 wt. % Ni Steel and its Weld Heat-Affected Zones, *Metallurgical and Materials Transactions A*, Vol. 49A, April 2018, pp. 1031-1043.
4. Erin J. Barrick, Divya Jain, John N. DuPont, and David N. Seidman, Effects of Heating and Cooling Rates on Phase Transformations in 10 Wt Pct Ni Steel and Their Application to Gas Tungsten Arc Welding, *Metallurgical and Materials Transactions A*, December 2017, Volume 48, Issue 12, pp 5890–5910.
5. Erin J. Barrick and John N. DuPont, Mechanical Properties and Microstructural Characterization of Simulated Heat-Affected Zones in 10 wt pct Ni Steel, *Materials Science and Engineering A*, Volume 748, 4 March 2019, Pages 189-204.
6. Erin J.Barrick and John N.DuPont, Microstructural characterization and toughness evaluation of 10 wt% Ni steel weld metal gas tungsten arc and gas metal arc weld fusion zones, Materials Science and Engineering: A, Volume 796, 7 October 2020, 140043.
7. Erin J.BarrickJohn N.DuPont, The influence of martensitic microstructure and oxide inclusions on the toughness of simulated reheated 10 wt% Ni steel weld metal multi-pass fusion zones, Materials Science and Engineering: A, Volume 801, 13 January 2021, 140336.
8. Kant, R., & DuPont, J. (2019). Stress Relief Cracking Susceptibility in High-Temperature Alloys. *Welding Journal*, *98*(2), 29-49. doi: 10.29391/2019.98.003.
9. Annor, M., Welding Metallurgy and Weldability and Weldability of Structural Fe-Mn Damping Steels [Thesis, Lehigh University].
10. DuPont, J., Robino, C., & Marder, A. (1999). Modelling mushy zones in welds of multicomponent alloys: implications for solidification cracking. *Science And Technology Of Welding And Joining*, *4*(1), 1-14. doi: 10.1179/stw.1999.4.1.1
11. Lippold, J.C. and Kotecki, D.J. (2005) “pg. 173-189,” in *Welding Metallurgy and weldability of Stainless Steels*. Hoboken, NJ: Wiley-Interscience.

APPENDIX A

A1 – Tables

Table 1. Composition of each 10 Ni alloy, HY-100, HY-130, 304 SS, and 310 SS. All values shown in weight percent.

Composition of Each Alloy (wt%)						
Element	**11334 Filler**	**11337 Filler**	**11705 Filler**	**HY-100 Base**	**304L Stainless Steel**	**310 Stainless Steel**
C	0.096	0.063	0.019	0.17	0.02	0.03
Mn	0.35	0.6	0.75	0.33	1.75	0.87
P	0.005	0.009	0.009	0.007	0.032	0.026
S	0.001	0.002	0.003	0.002	0.023	0.002
Si	0.35	0.34	0.46	0.21	0.35	0.53
Ni	9.42	9.43	9.43	2.39	8.29	19.17
Cr	0.01	0.01	0.01	1.26	18.26	25.66
Mo	1.16	1.15	0.66	0.23	0.45	0.14
Cu	0.01	0.01	0.01	0.16	0.51	0.17
Ti	0.01	0.01	0.01	<0.01	<0.01	0.01
Al	0.01	0.01	0.01	0.02	<0.01	0.01
V	0.14	0.14	0.18	<0.01	0.07	0.07
Co	0.01	0.01	0.01	N/A	0.13	0.20
Nb	0.01	0.01	0.01	N/A	N/A	N/A
Zr	0.01	0.01	0.01	N/A	N/A	N/A
Fe	Balance	Balance	Balance	Balance	Balance	Balance

Table 2. Parameters used to make gas metal arc welds with the 11334, 11337, and 11705 filler metals.

Shield Gas Details	
Shield Gas Composition	98% Ar, 2% O_2
Target Flow Rate (cubic feet per hour)	40 - 45
Nozzle Diameter (inches)	0.625
Set-Up Details	
Welding Position	Groove, Flat
Base Material	HY-100
Material Thickness (inches)	1
Bevel Angle (degrees)	22.5
Root Opening (inches)	0.5
Welding Instructions	
Current Range (amps)	250 - 280
Voltage Range (V)	24 - 26
Heat Input Range (kJ/inch)	40 - 45
Travel Speed (inches per minute)	10-12
Number of Passes	20
Number of Layers	7
Preheat/Interpass Temperature	
Min. Preheat Temperature (°F)	250
Interpass Temperature (°F)	250 - 275

Table 3. SEM parameters used to obtain SRC fracture surface images.

Aperture (µm)	30
Accelerating Voltage (kV)	20
Working Distance (mm)	20

Table 4. Assigned values of 'severity' and 'detectability' for all susceptibility parameters. Below each value is the range used in sensitivity analysis.

Material/ Temp	Ductility (P1)	% Stress Relaxed (P2)	Hardness at fracture (P3)	Failure time (P4)	Fracture Mode (P5)	Intergranular Secondary Cracks (P6)
Severity (x/10) -Effect on output	**8**	**8**	**6**	**10**	**10**	**10**
Detectability (x/10) -Ease of detection	**10**	**10**	**10**	**10**	**8**	**8**

A2 – Figures

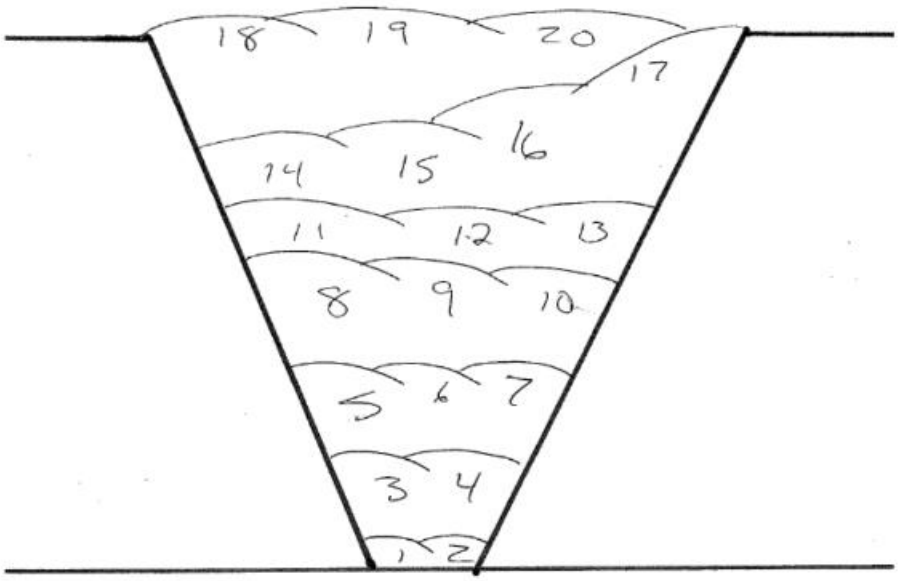

Figure 1. Groove joint design for the welded test plates and schematic of each pass.

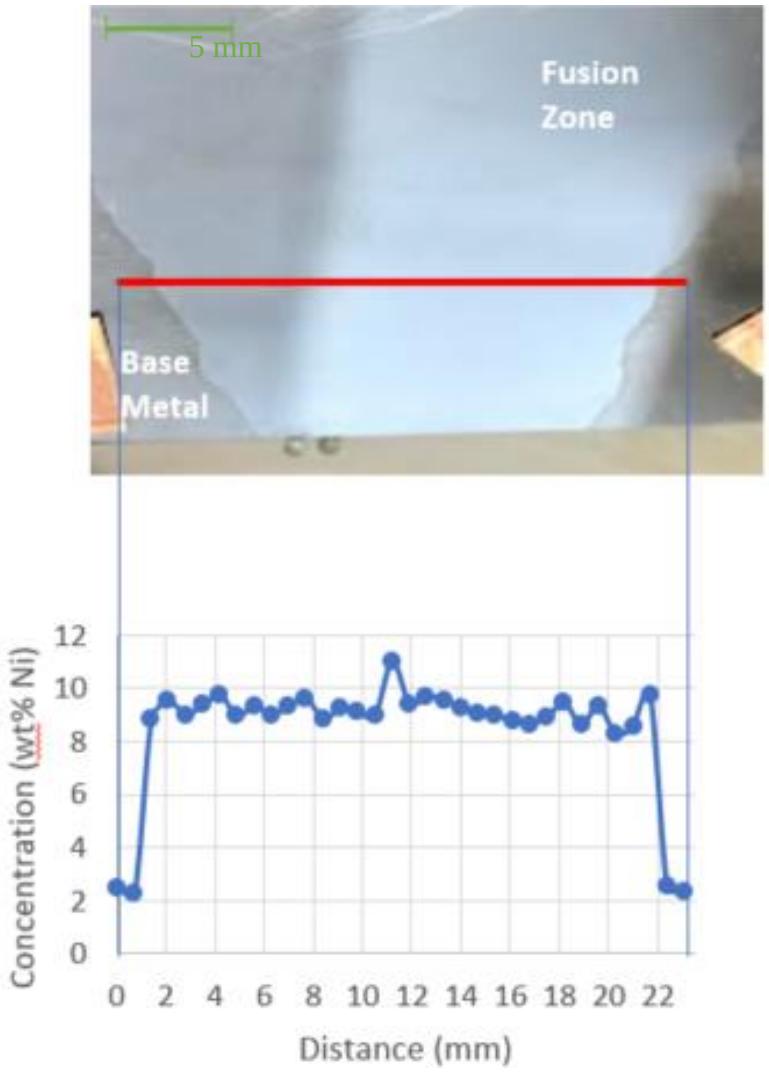

Figure 2. Ni concentration at various points across the cross section of the weld made with 11337 filler material.

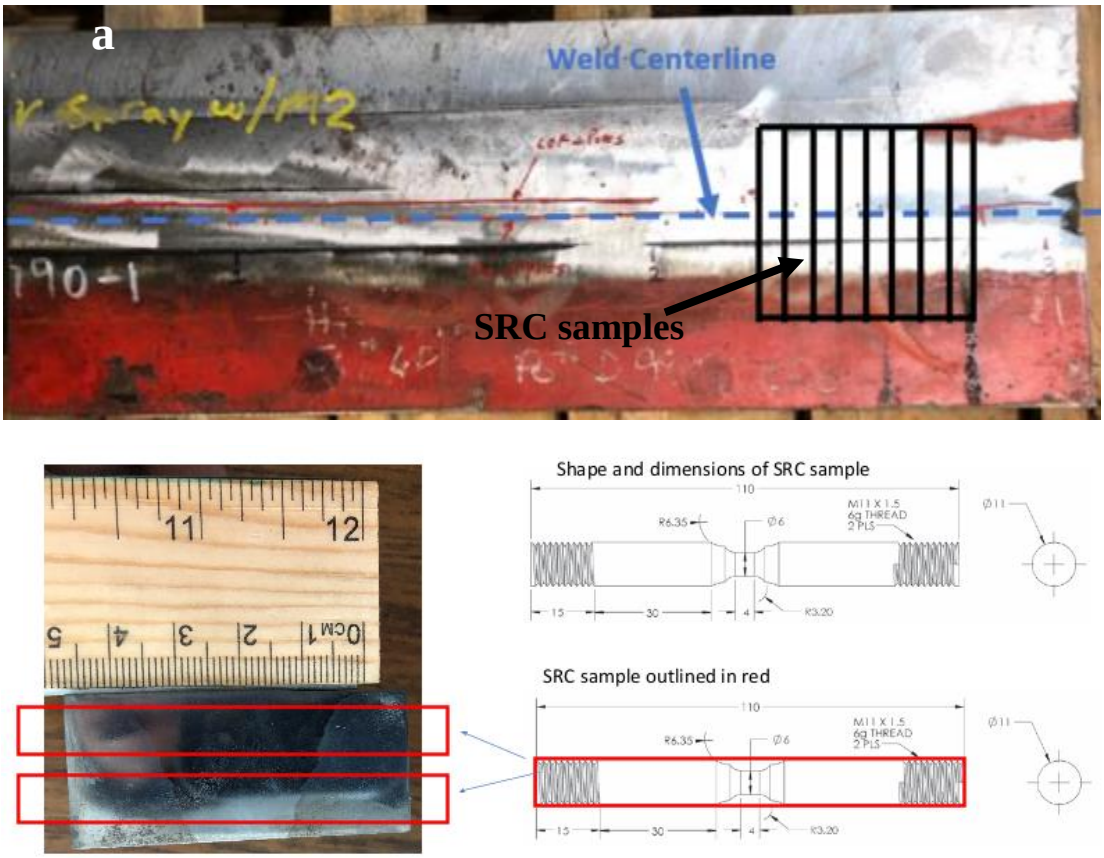

Figure 3. (a) Welded plate with the orientation of the extracted SRC samples and (b) dimensions of the samples.

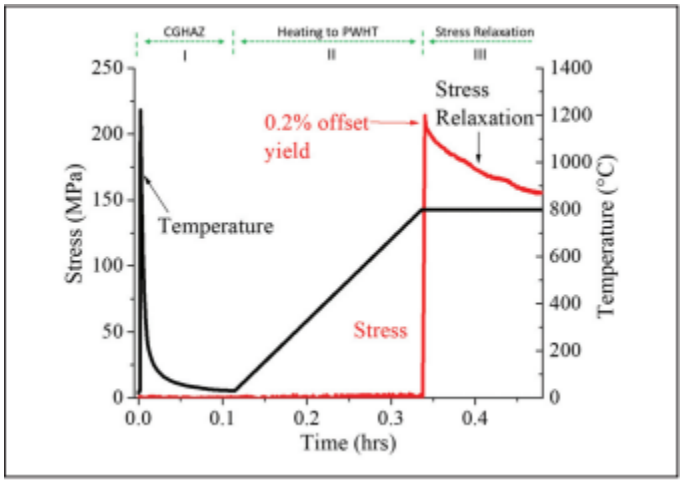

Figure 4. Stress and Temperature vs. Time during a typical stress relief cracking test; 0.2% strain offset.

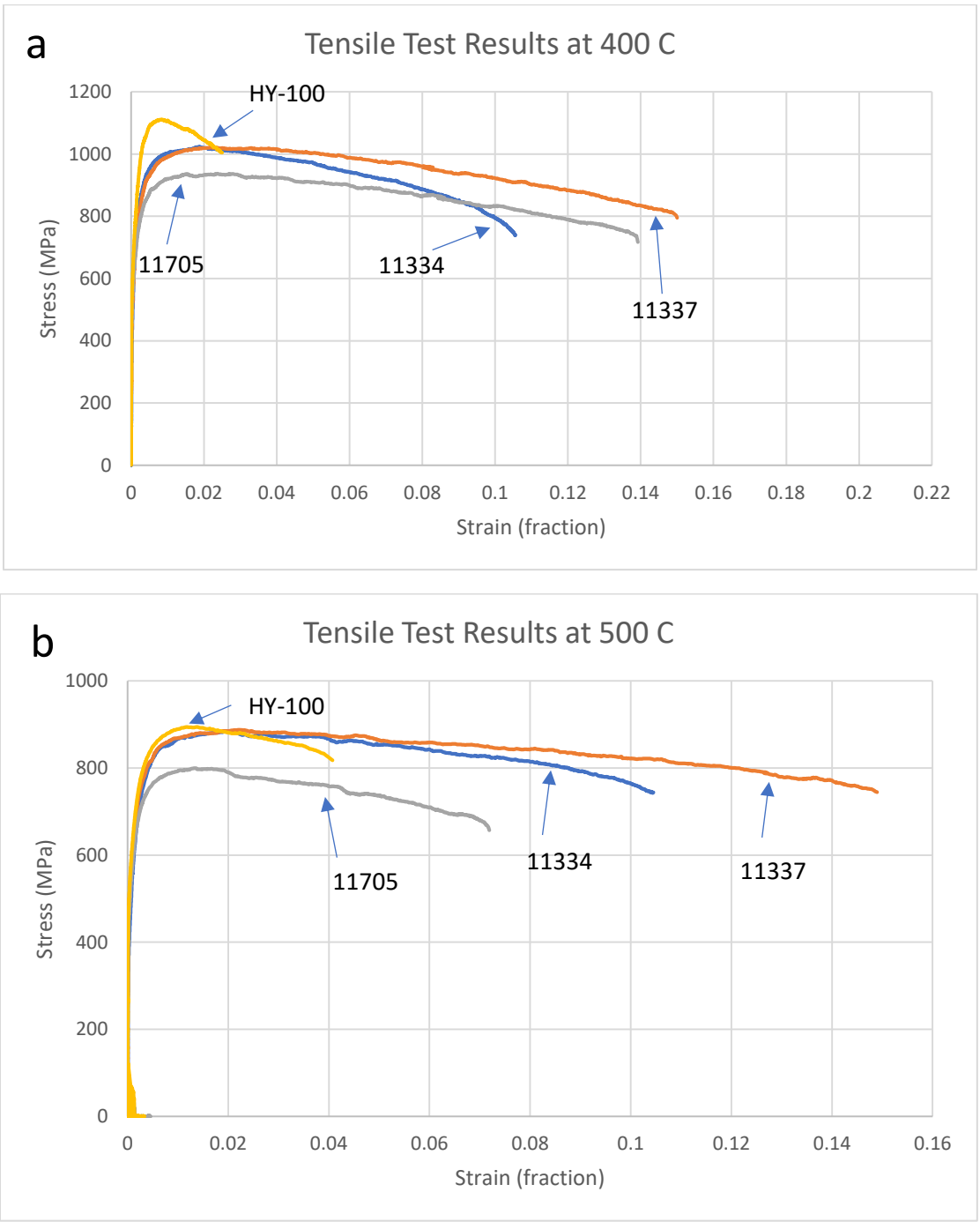

Figure 5. Tensile test results of each alloy at (a) 400 ˚C, (b) 500 ˚C, (c) 600 ˚C, and (d) 700 ˚C.

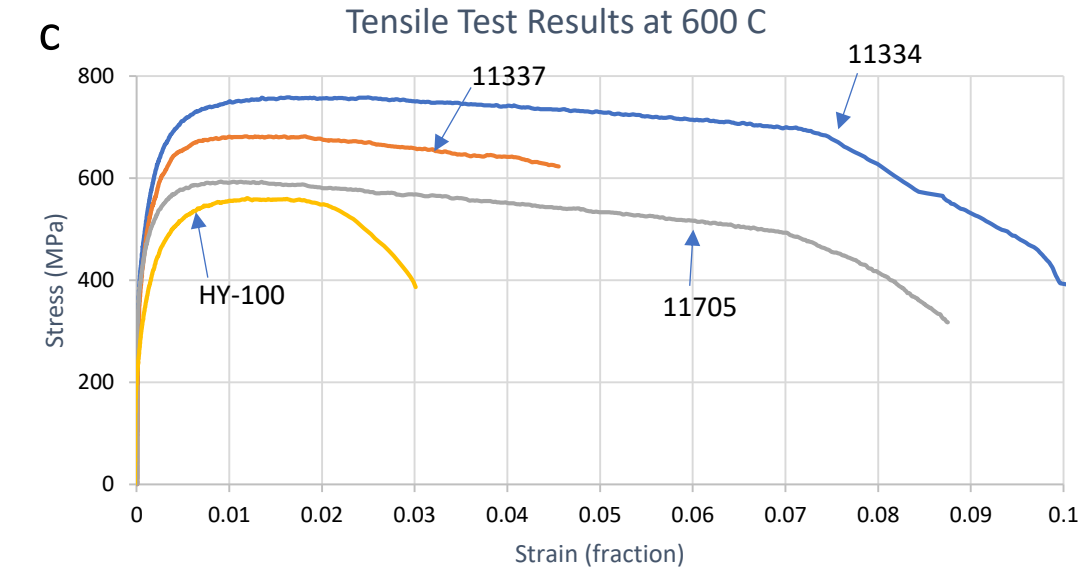

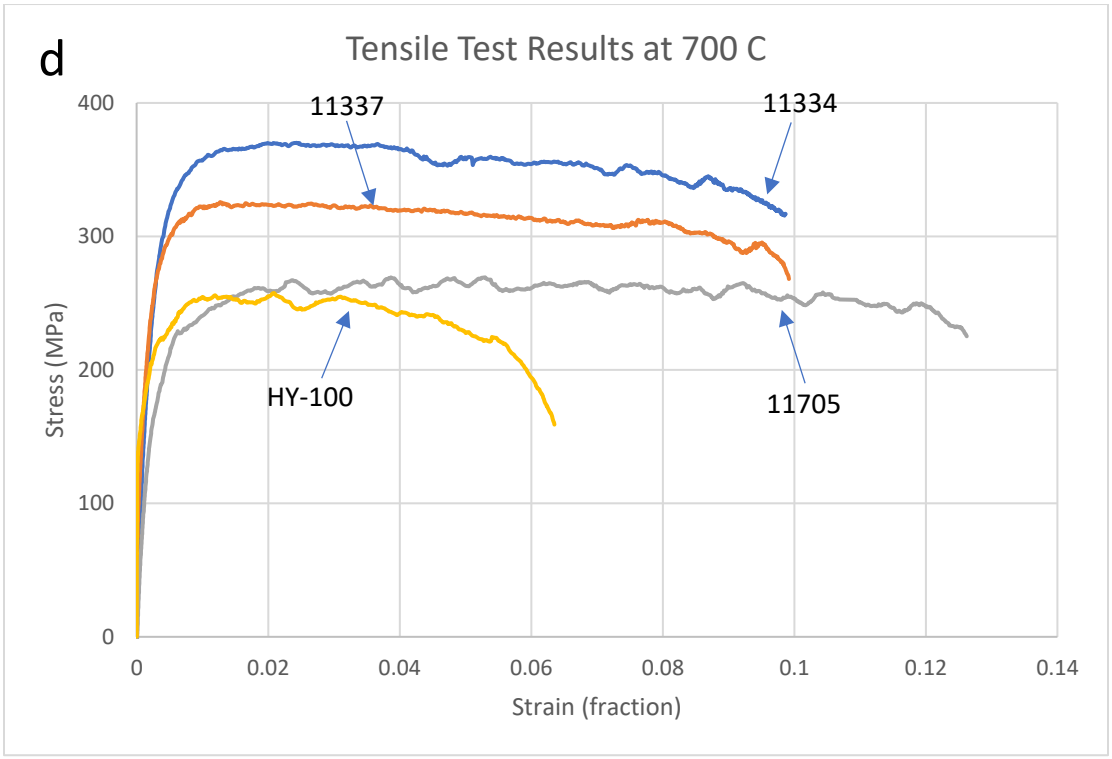

Figure 5 (continued). *Tensile test results of each alloy at (a) 400 ˚C, (b) 500 ˚C, (c) 600 ˚C, and (d) 700 ˚C.*

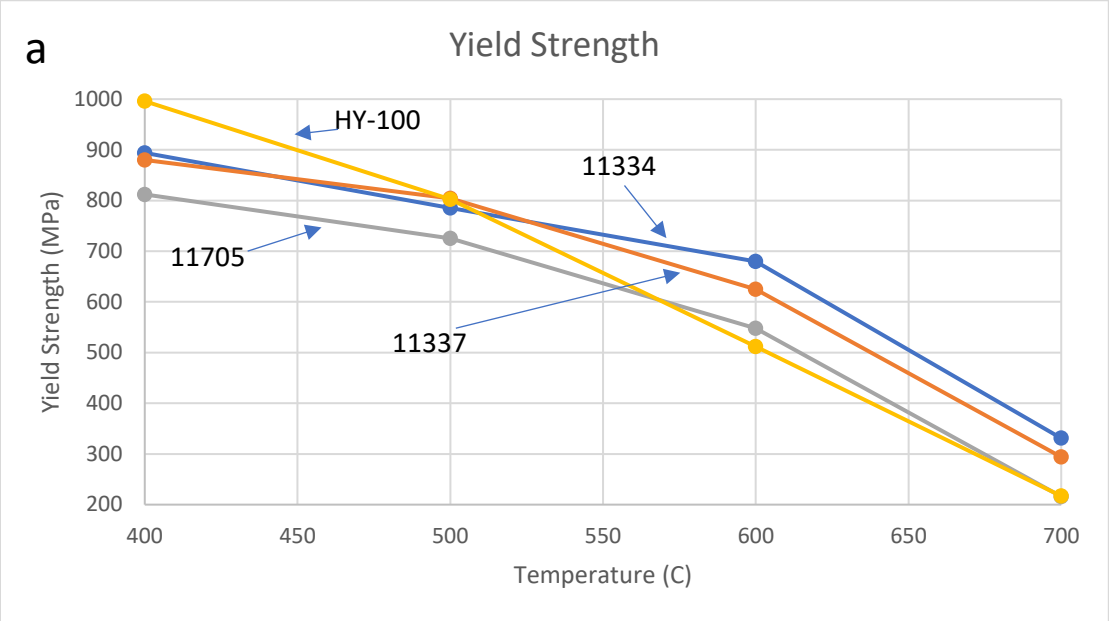

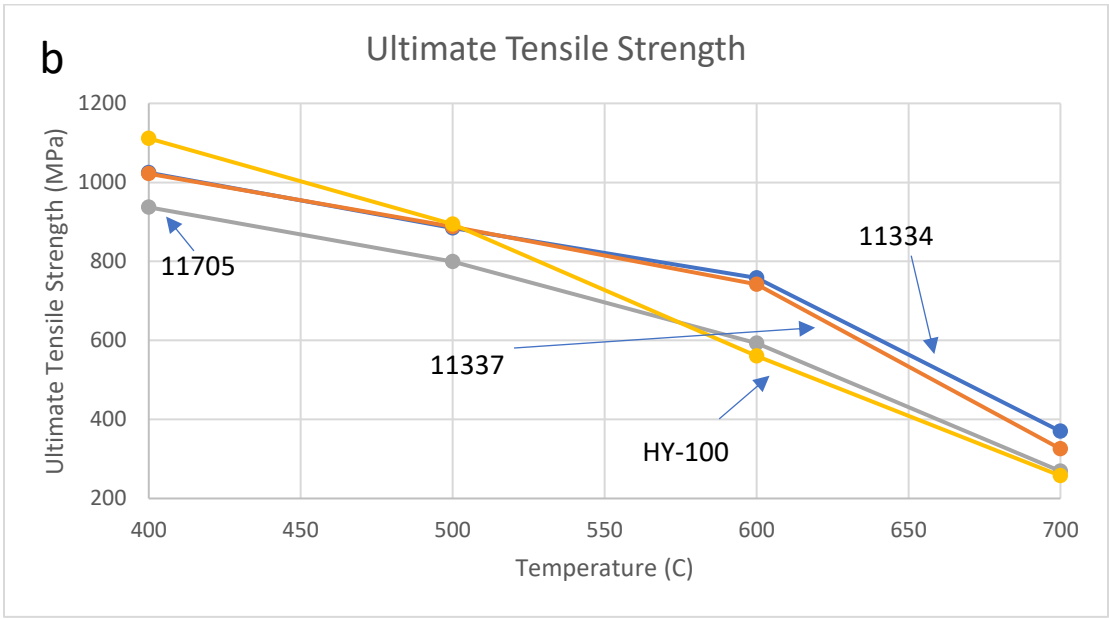

Figure 6. Plot of (a) yield strength, (b) tensile strength, and (c) reduction in area as functions of temperature for each alloy. Results obtained from hot temperature tests.

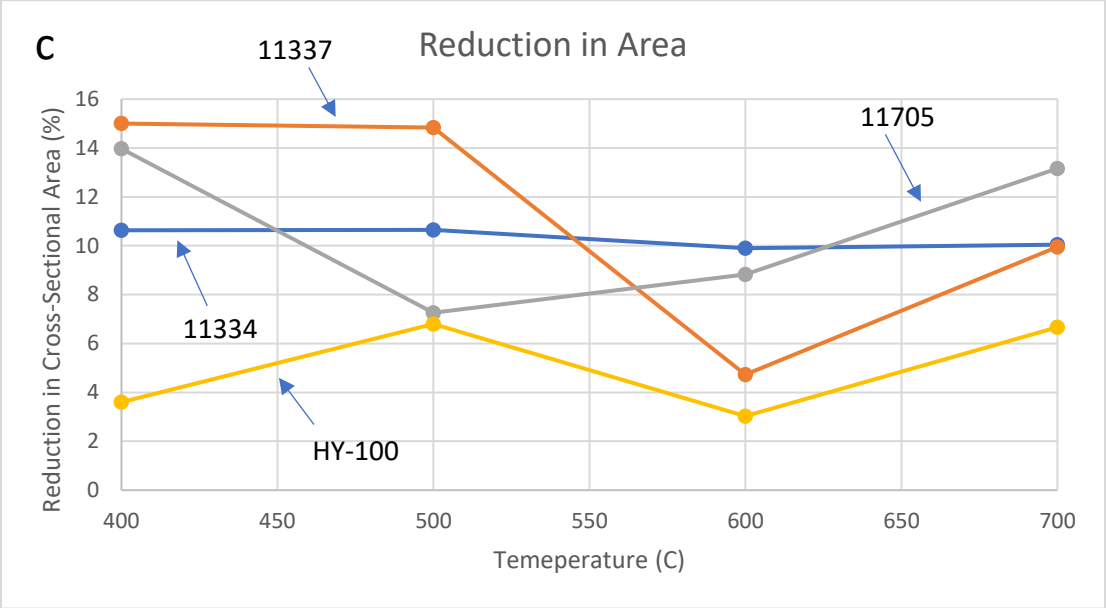

Figure 6 (continued). Plot of (a) yield strength, (b) tensile strength, and (c) reduction in area as functions of temperature for each alloy. Results obtained from hot temperature tests.

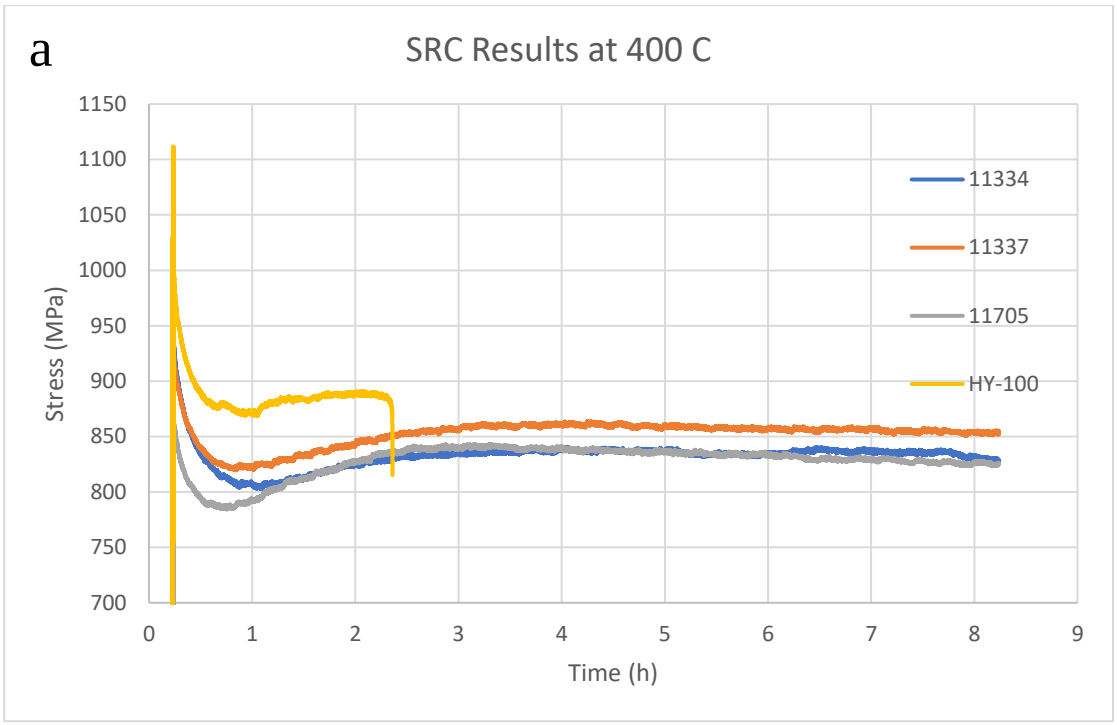

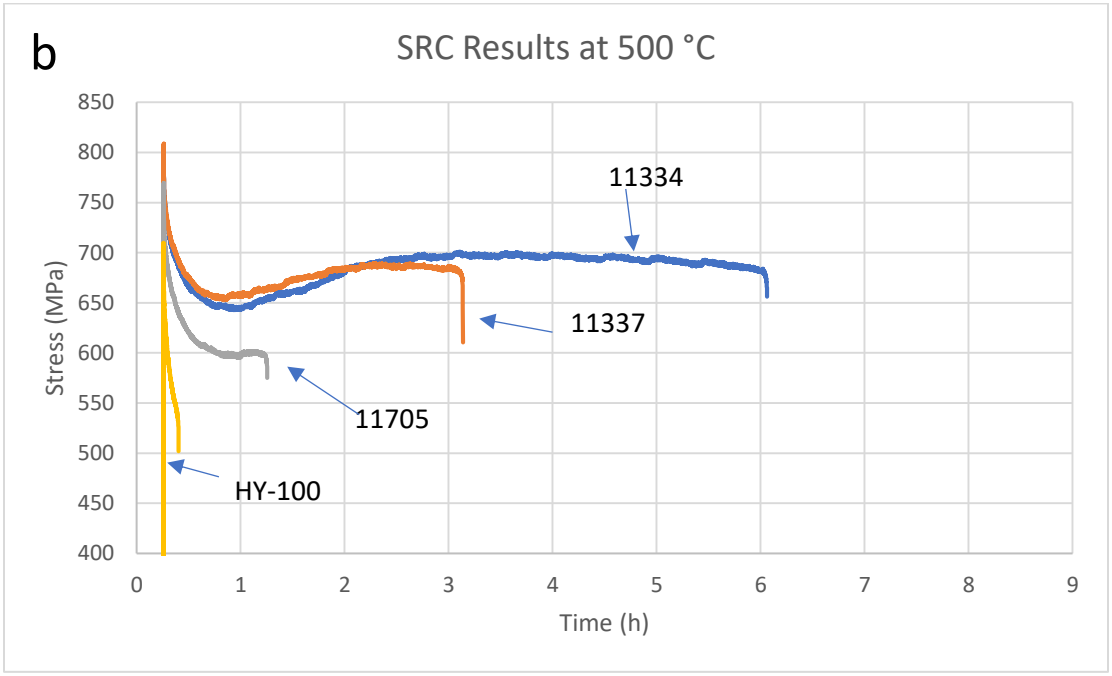

Figure 7. Stress vs. Time plots of stress relief cracking tests at (a) 400 ˚C, (b) 500 ˚C, (c) 600 ˚C, (d) a closeup of the curves at 600 ˚C, and (e) 700 ˚C.

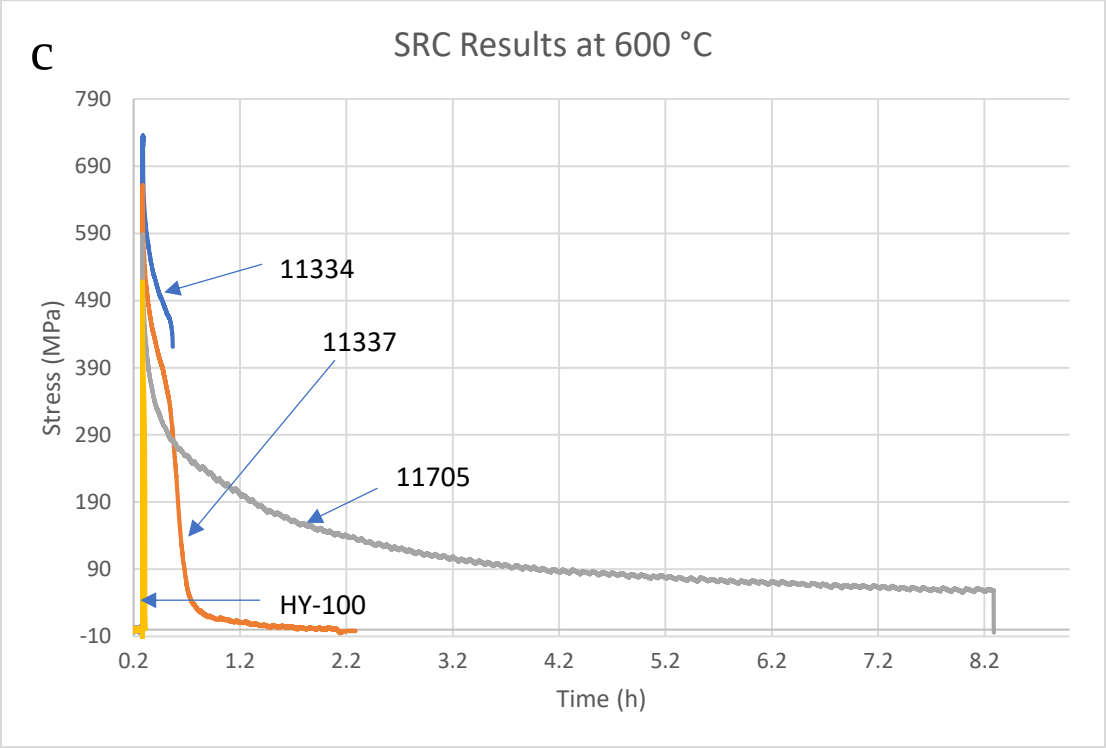

Figure 7 (continued). Stress vs. Time plots of stress relief cracking tests at (a) 400 ˚C, (b) 500 ˚C, (c) 600 ˚C, (d) a closeup of the curves at 600 ˚C, and (e) 700 ˚C.

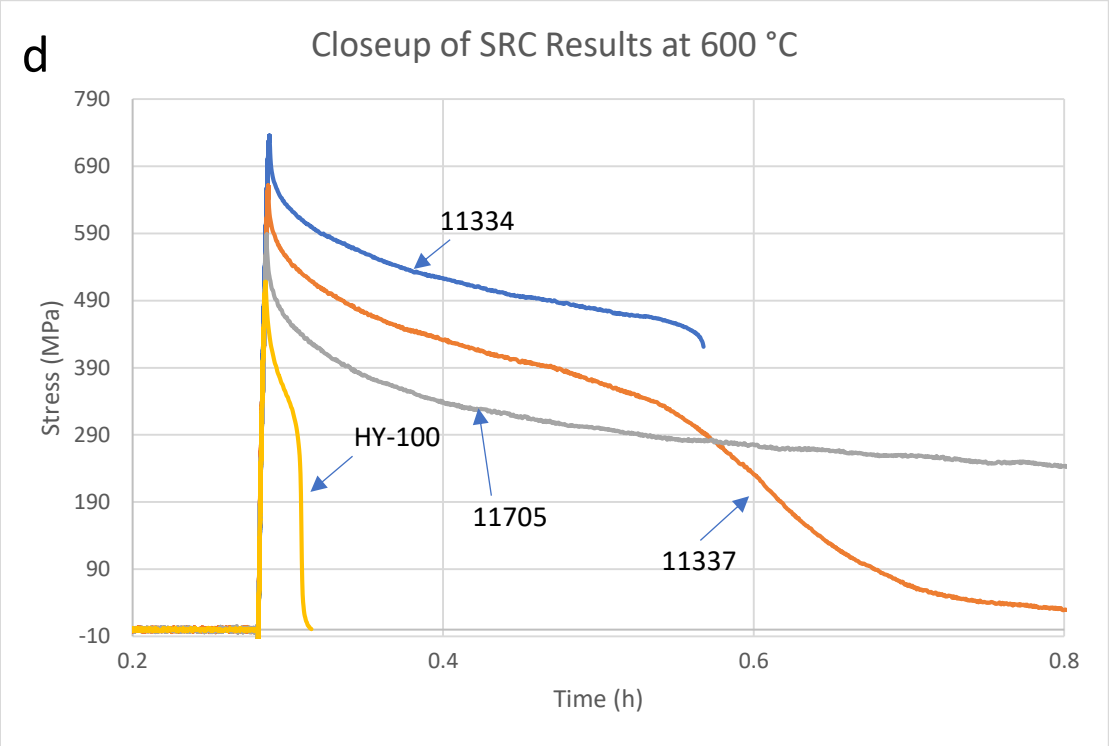

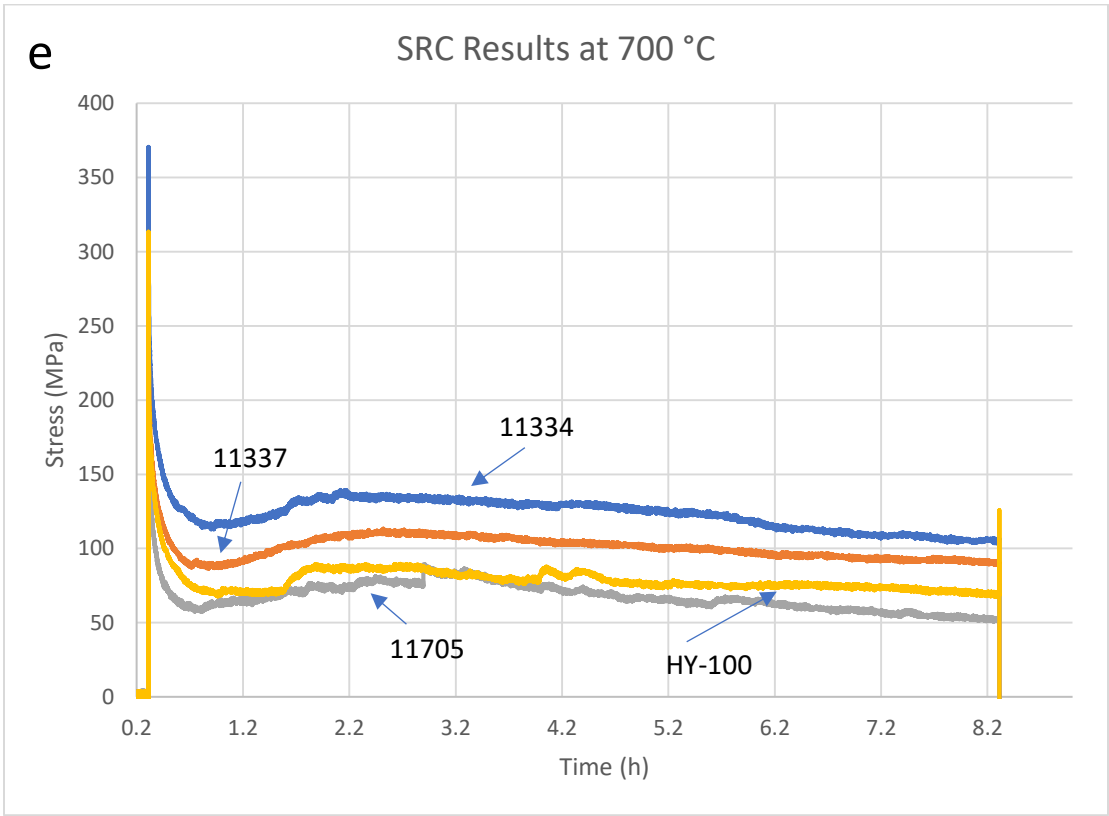

Figure 7 (continued). *Stress vs. Time plots of stress relief cracking tests at (a) 400 ˚C, (b) 500 ˚C, (c) 600 ˚C, (d) a closeup of the curves at 600 ˚C, and (e) 700 ˚C.*

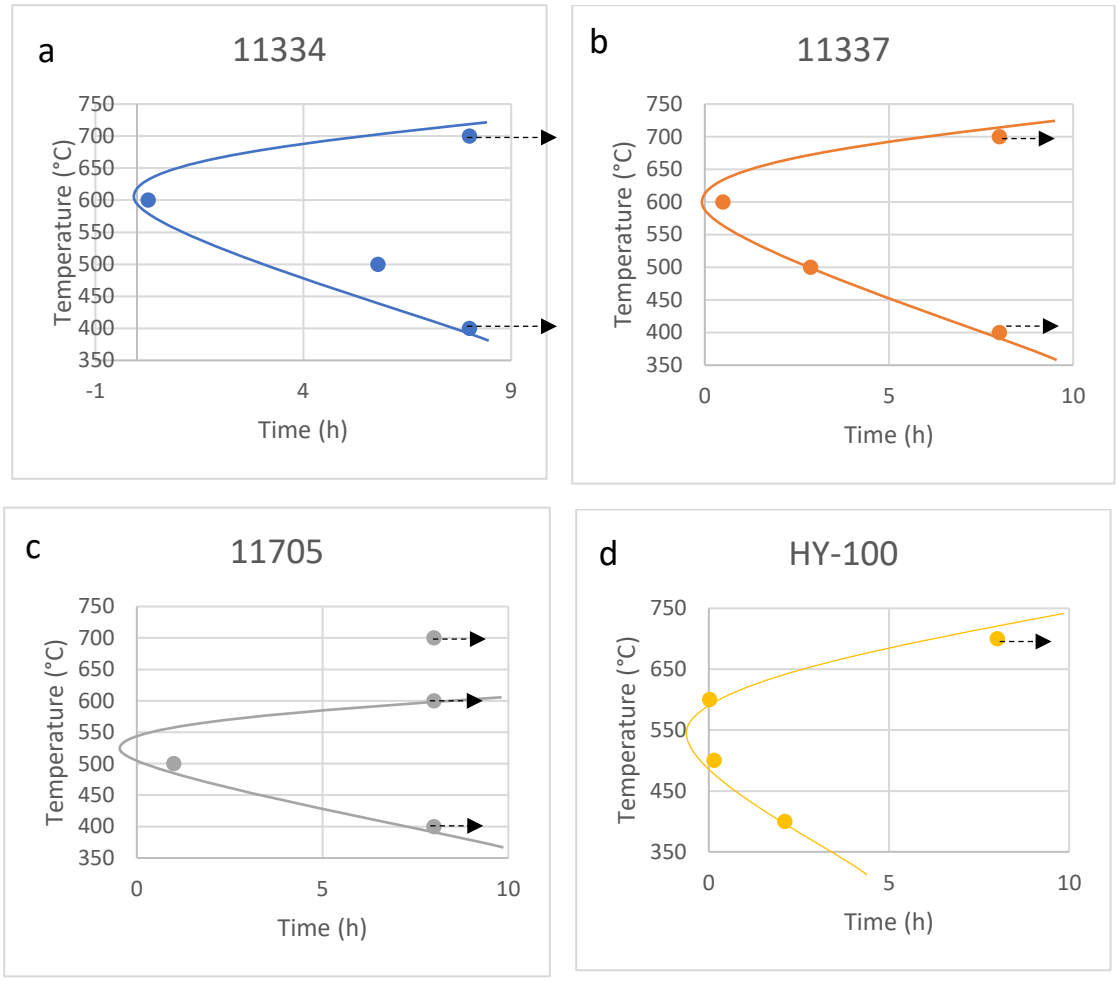

Figure 8. Post weld heat treatment Temperature vs. Time to failure with fitted "C" curves for alloys (a) 11334, (b) 11337, (c) 11705, and (d) HY-100.

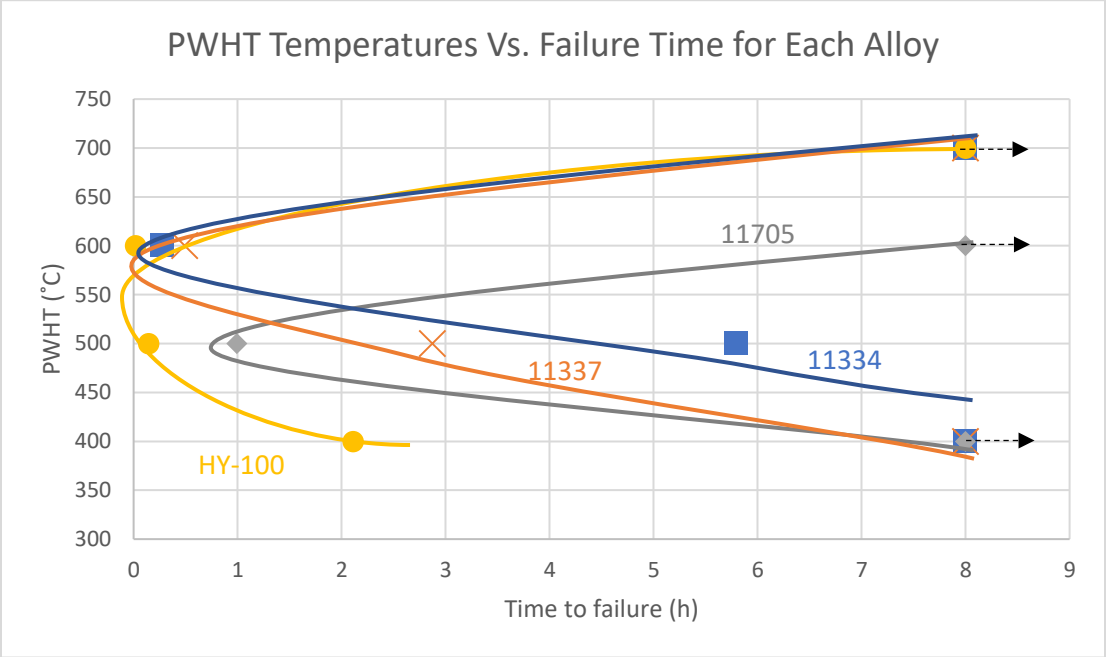

Figure 9. Post weld heat treatment temperature vs. Time to Failure of all four alloys.

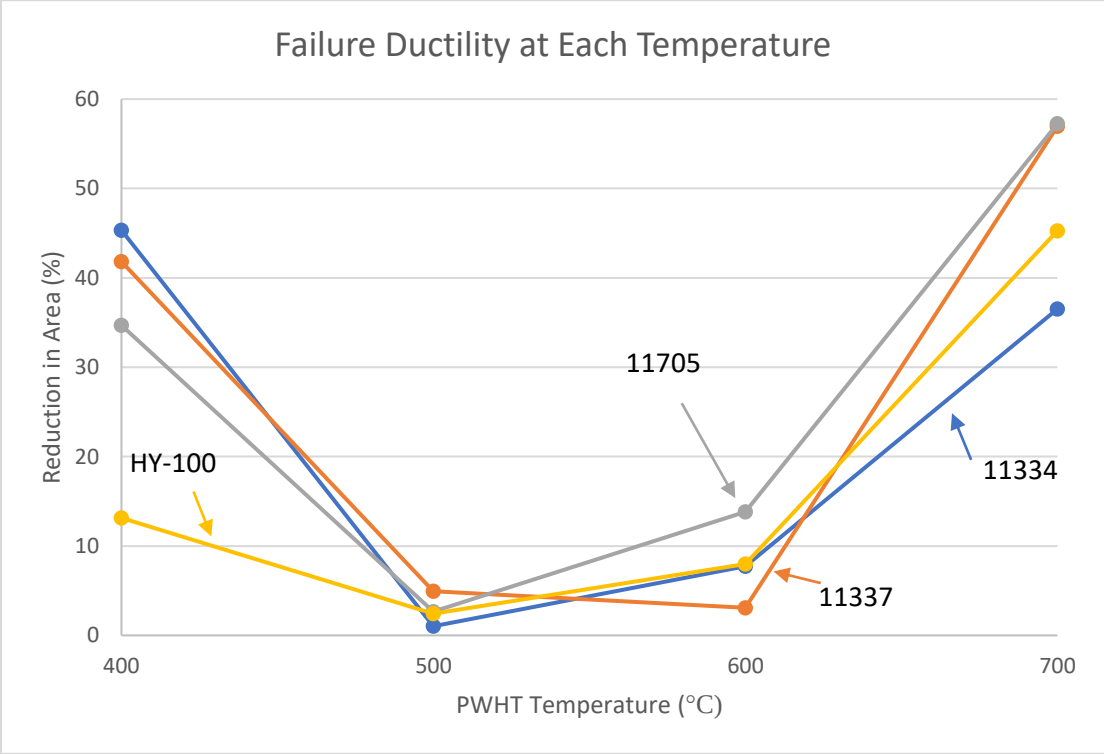

Figure 10. Reduction in area of sample after testing.

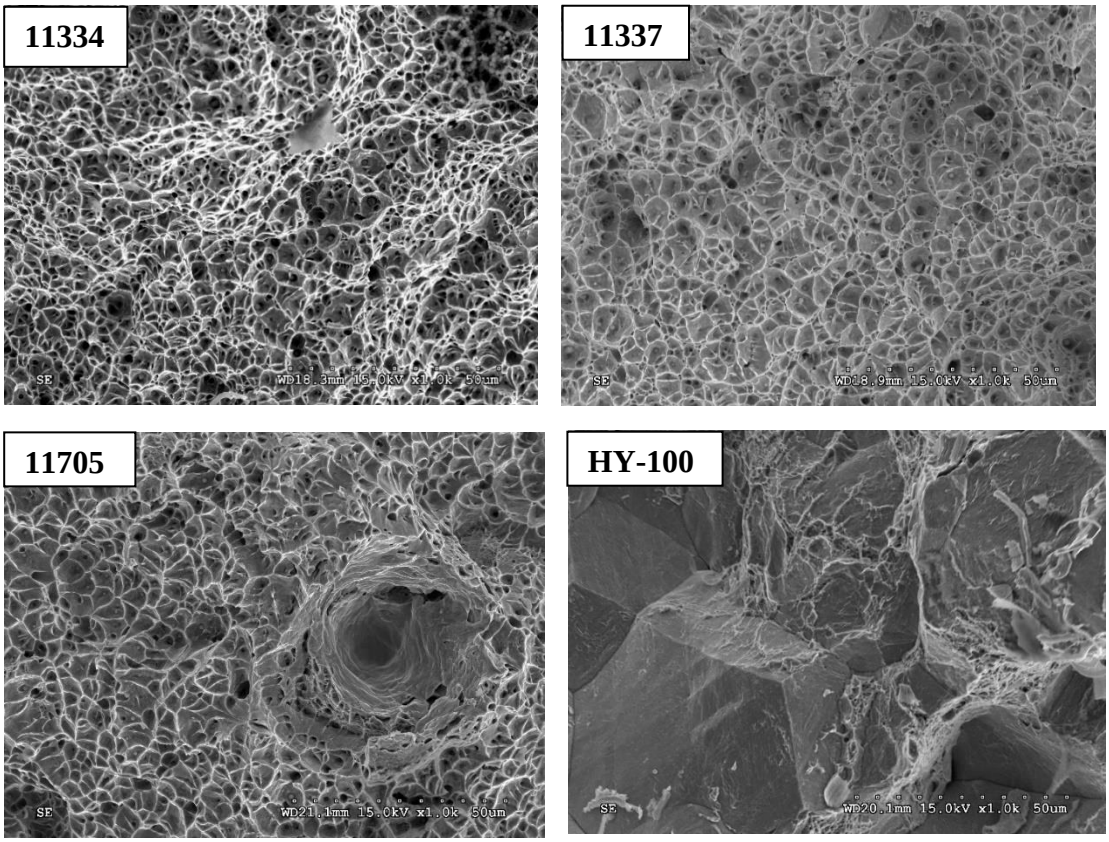

Figure 11. Fracture surface images of each sample at a post weld heat treatment temperature of 400 ˚C.

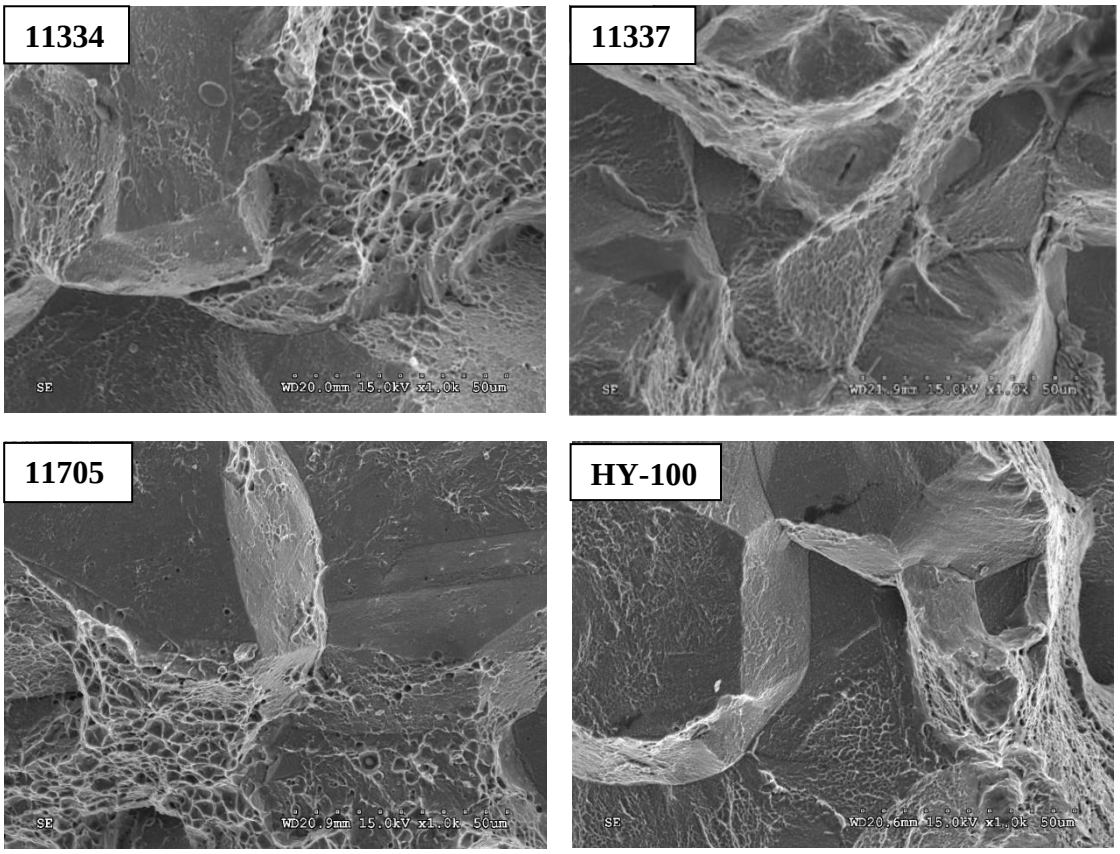

Figure 12. Fracture surface images of each sample at a post weld heat treatment temperature of 500 ˚C.

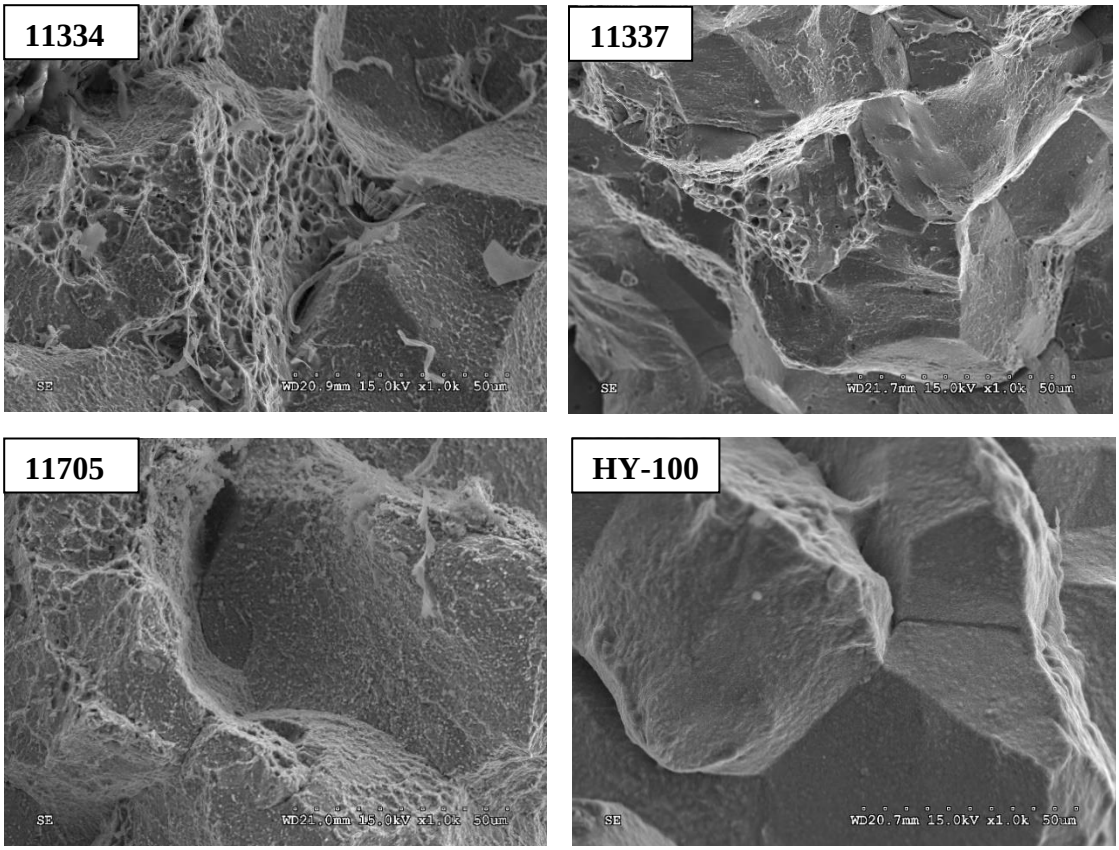

Figure 13. Fracture surface images of each sample at a post weld heat treatment temperature of 600 ˚C.

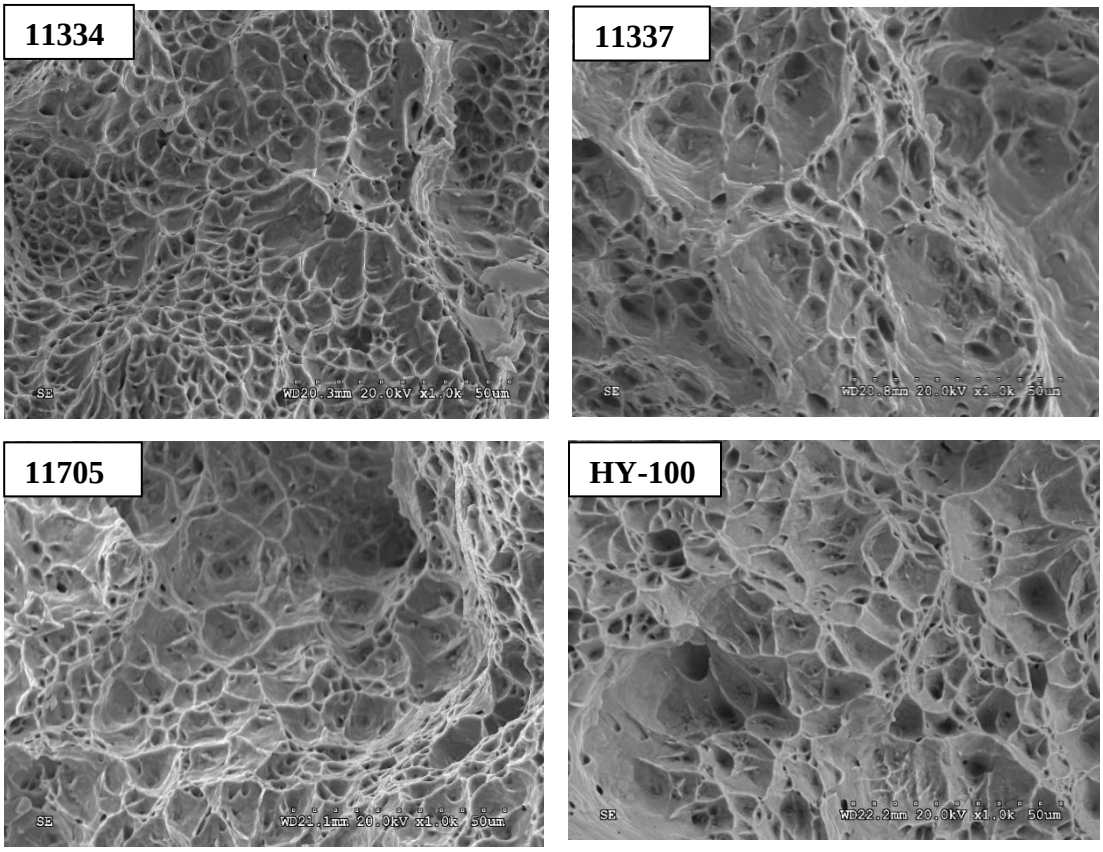

Figure 14. Fracture surface of images of each sample at a post weld heat treatment temperature of 700 °C.

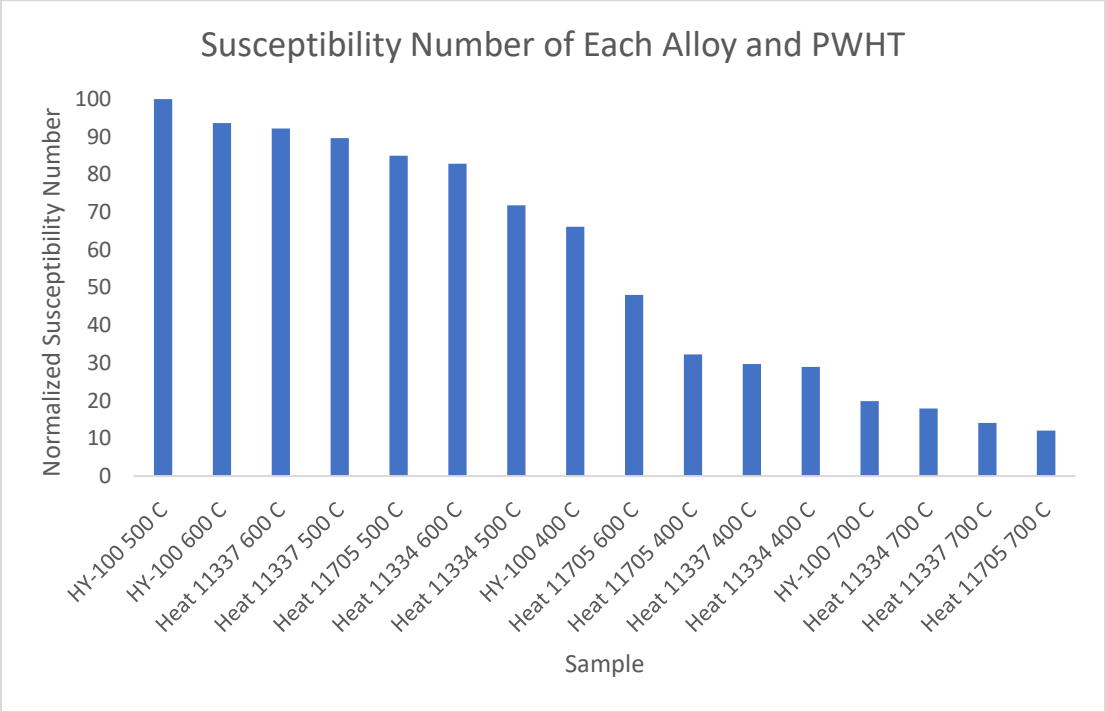

Figure 15. Normalized susceptibility number for each sample.

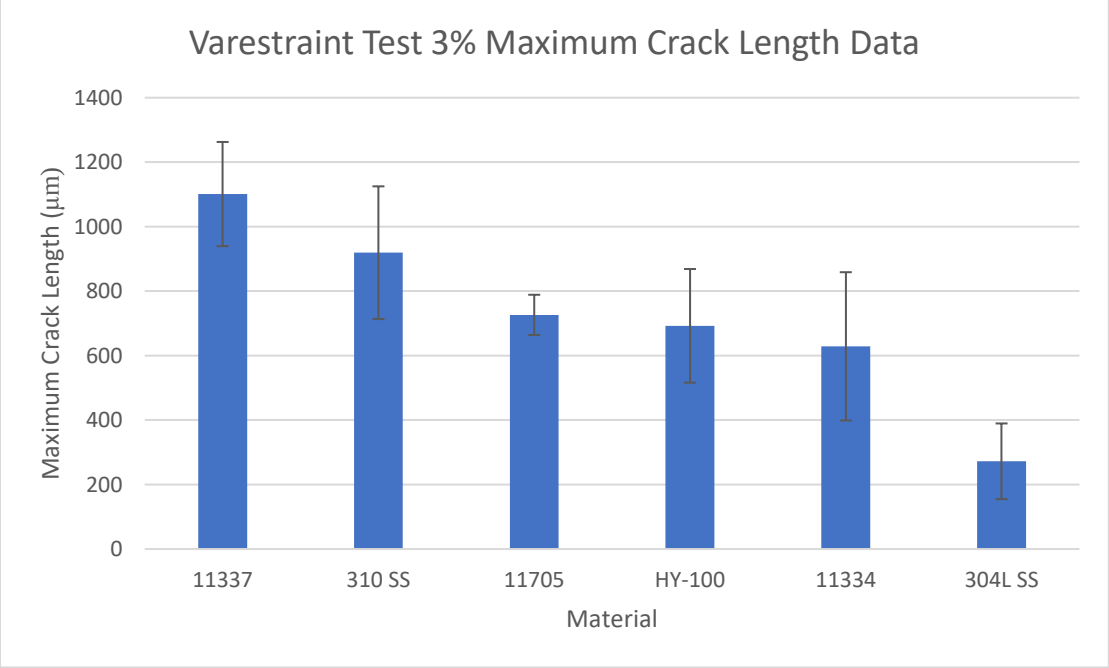

Figure 16. Varestraint Results of each composition of 10 wt% Ni, the HY-100 alloy, SS grade 310 and SS grade 304L. Three to four replicas were tested on each composition/alloy.

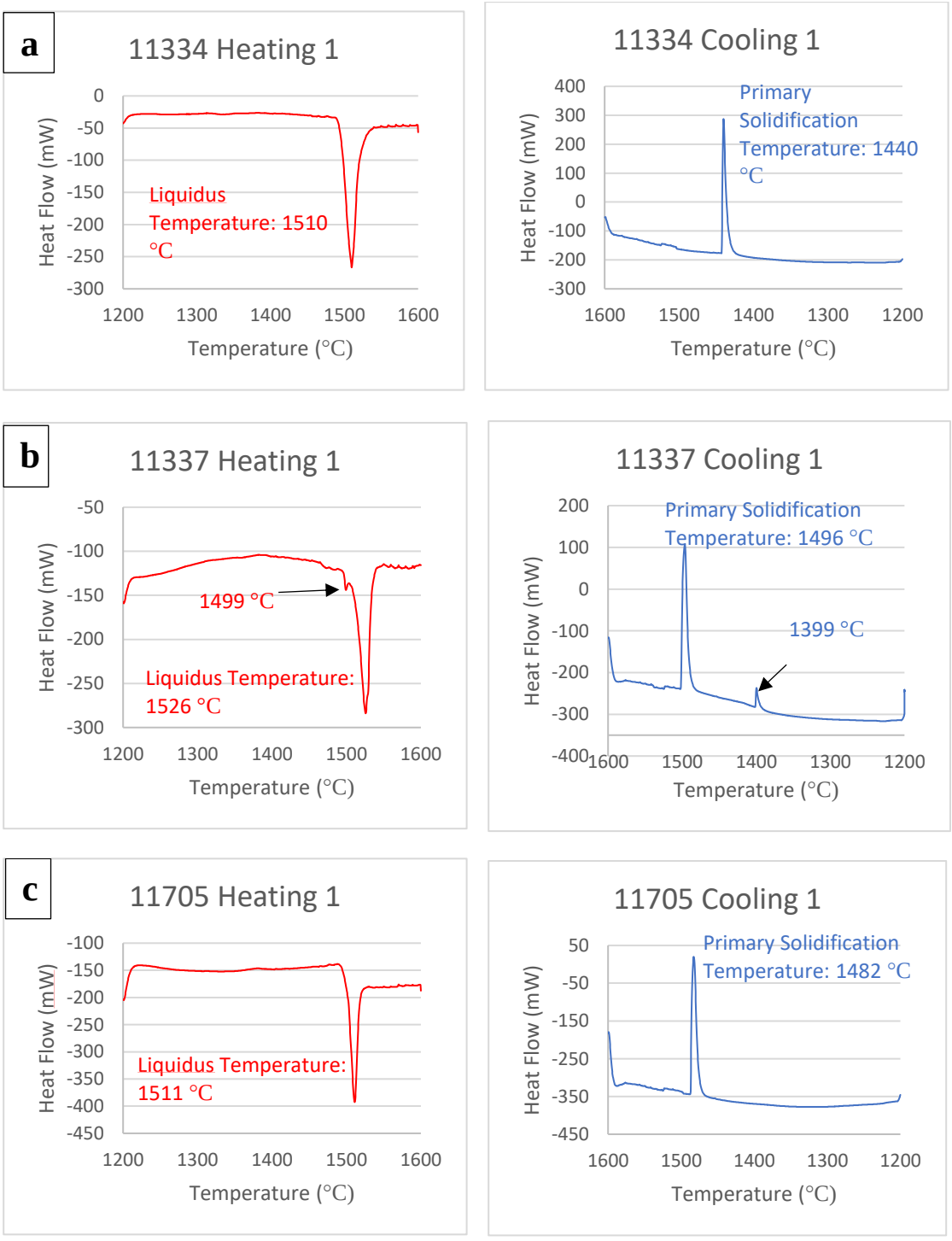

Figure 17. On-heating and on-cooling differential scanning calorimetry curves of 10 Ni alloys (a) 11334, (b) 11337, (c) 11705, and (d) HY-100 base material.

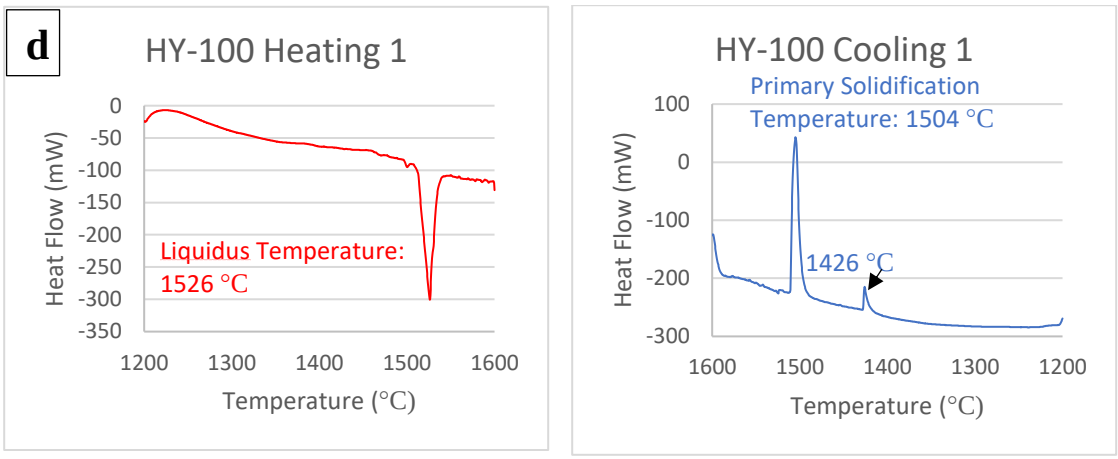

Figure 17 (continued). On-heating and on-cooling differential scanning calorimetry curves of 10 Ni alloys (a) 11334, (b) 11337, (c) 11705, and (d) HY-100 base material.

APPENDIX B/BIO

Nicholas L. Yang was born in Boston, Massachusetts on May 10th, 1999. He attended high school in Tyngsboro, MA and enrolled at Lehigh University to later receive a Bachelor of Science degree in May 2021 and a Master of Science in May 2023, both in materials science and engineering.